Taylor & Francis
Taylor & Francis Group

Structure and Infrastructure Engineering
Maintenance, Management, Life-Cycle Design and Performance

ISSN: 1573-2479 (Print) 1744-8980 (Online) Journal homepage: https://www.tandfonline.com/loi/nsie20

Parameterized seismic life-cycle cost evaluation method for building structures

Mohamed Noureldin & Jinkoo Kim

To cite this article: Mohamed Noureldin & Jinkoo Kim (2020): Parameterized seismic life-cycle cost evaluation method for building structures, Structure and Infrastructure Engineering, DOI: 10.1080/15732479.2020.1759656

To link to this article: https://doi.org/10.1080/15732479.2020.1759656

Published online: 12 May 2020.

STRUCTURE AND INFRASTRUCTURE ENGINEERING
https://doi.org/10.1080/15732479.2020.1759656

Parameterized seismic life-cycle cost evaluation method for building structures

Mohamed Noureldin and Jinkoo Kim

Department of Civil and Architectural Engineering, Sungkyunkwan University, Suwon, Korea

ABSTRACT

A framework for seismic life-cycle cost (LCC) evaluation is proposed for low to mid-rise framed buildings based on structural fundamental response quantities such as stiffness, strength, and ductility. The LCC is calculated using simple formulas for a basic reference model (BRM) with assumed fundamental response quantities after it is transformed into an equivalent single degree of freedom (ESDOF) system. The pushover curves of the target structure and the BRM are compared and the difference in each response quantity is related to the LCC using the set of the prepared graphs. Then, the final LCC is calculated using the LCC of the BRM and the differences in LCC due to the difference in each response quantity. The effectiveness of the proposed method is verified through comparison with the results from a rigorous method based on nonlinear time history analysis. The results of the analysis turn out to show reasonable agreement with those obtained from the rigorous method, and it is concluded that the parameterized LCC proposed in this study is an easy and practical tool for estimating LCC using fundamental response quantities of low to mid-rise buildings.

ARTICLE HISTORY
Received 21 August 2019
Revised 6 December 2019
Accepted 7 January 2020

KEYWORDS
Damage state probability; fragility analysis; life-cycle cost; loss assessment; seismic hazard; buildings; equivalent system

1. Introduction

Recently, there has been growing interests in the research on life-cycle cost (LCC) evaluation of structures since it has become one of the important factors of the performance-based design as well as optimization of decisions related to maintenance and retrofit of structures (Pandey & Weide, 2017). In addition, researchers have broadened the scope of LCC analysis beyond earthquakes to include other natural hazard risks such as hurricanes, energy consumption or wind. For seismic hazard, it has been applied not only to main-shock events but also to the after-shock events, which may increase the life-cycle earthquake-induced losses by up to 30%.

Some research attempts have focused on the practical side of the probabilistic loss assessment, which is an important step in LCC. For example, a practice-oriented probabilistic approach for the seismic performance assessment of building structures using the SAC-FEMA approach and the pushover-based N2 method has been proposed by Fajfar and Dolsek (2012). Sullivan, Welch, and Calvi (2014) presented simplified tools for risk assessment, such as the simple definition of collapse fragility, based on FEMA P-58 guidelines (2012) and applied them to a benchmark 4-story building. Welch, Sullivan, and Calvi (2014) extended the direct displacement-based assessment to consider probabilistic aspects in a simplified fashion. They applied the approach to four and eight-story RC building examples and concluded that future researches are needed for different structural configuration and retrofitting of non-ductile buildings. Kosič, Fajfar, and Dolsek (2014) presented a seismic risk assessment based on pushover analysis. They proposed a probabilistic SDOF model to incorporate uncertainty analysis. Four building samples were tested and their seismic risk was estimated with reasonable accuracy. Kosič, Dolsek, and Fajfar (2016) conducted an extensive study on different types of low to medium-height RC buildings to obtain the dispersion values required for pushover-based risk assessment.

Recently, studies on the simplification of the LCC evaluation have been carried out. For example, Esteva, Díaz-López, Vásquez, and León (2016) studied the seismic vulnerability function and its relation with the damage accumulation, and presented some rough estimations for the accumulated damage of buildings. In addition, they investigated the optimum values of the damage threshold required for retrofitting structures. Noureldin and Kim (2017) used a simple loss estimation procedure to develop a practical seismic life-cycle cost methodology for steel jacket offshore platforms. Liu and Mi (2017) calculated the future cost of the repair/replacement of earthquake-damaged energy-efficiency features in buildings through a simple method considering the seismic hazard analysis. Vitiello, Asprone, Di Ludovico, and Prota (2017) developed a simplified method based on a semi-probabilistic methodology to evaluate the economic performance of a building prone to seismic risk. The proposed approach aimed to identify the most cost-effective strengthening strategies through optimal strengthening levels for existing structures during their structural lifetime.

Bojórquez, Ruiz, Ellingwood, Reyes-Salazar, and Bojórquez (2017) proposed a method for establishing optimal seismic load factors for limit state design of buildings

CONTACT Jinkoo Kim jkim12@skku.edu

to achieve a minimum total expected life-cycle cost while maintaining the mean annual failure rate less than a prescribed value. El-Khoury, Shafieezadeh, and Fereshtehnejad (2018) introduced a risk-based LCC optimal control algorithm, where LCC is incorporated as the performance objective in the control design. In addition, the study introduced a risk-based probabilistic framework for LCC analysis of existing and proposed control strategies. Noureldin, Kim, and Kim (2019) applied a simplified LCC method for optimum design of an energy dissipation device for seismic retrofit of a structure. Mirzaei and Nasserasadi (2019) proposed a fast seismic LCC by employing a fast method for developing the fragility function based on genetic-algorithm optimization. Zhu et al. (2019) proposed a seismic risk & loss assessment procedure for the quantitative estimation of the LCC of industrial buildings located in China. The LCC is examined on the basis of stochastic simulation with the big data of building damage sampling.

Despite the recent computational and analytical advances, the concepts of LCC are far from being explicitly addressed in design codes and effectively implemented into practice. Del Gobbo et al. (2018) suggested that modern building standards do not reliably deliver earthquake resilience. The main reason is attributed to the high repair costs that follow a severe earthquake that may lead to demolishing the entire building. This makes the inclusion of the LCC in the early design stage crucial. Therefore, more research effort is needed to fill the gap between theory and practice by incorporating life-cycle concepts in structural design codes. An effort is currently ongoing within the Structural Engineering Institute (SEI)/ASCE to meet this need (Biondini & Frangopol, 2016). Behrouz (2019) raised some concerns in his study regarding using a design-based earthquake to obtain minimum LCC for steel moment-resisting structures. His study revealed that the design-basis-earthquake needs to be increased by at least 40% to achieve the minimum LCC. FEMA P-58 (2012) provides practical tools for LCC assessment of buildings; however, to practically implement them in building design, engineers need simplified tools to develop preliminary designs that approximately meet the desired performance level (Hamburger, Rojahn, & Heintz, 2012).

Despite many recent LCC studies, there still is a lack of studies that investigate the relationship between LCC and the main input structural parameters of the building, such as strength, stiffness, and ductility. The main purpose of the current study is to provide a practical tool that can provide preliminary LCC estimation with reasonable accuracy based on the main input structural parameters of the building. The effect of these input structural parameters on the LCC is investigated and simplified relationships are proposed to relate these input parameters with LCC. The parameterized LCC tool proposed in this paper is intended for selecting among different retrofitting interventions related to stiffness, strength, or ductility based on their expected LCC. On the other hand, for a newly designed building, it can be used for a quick LCC estimation of different alternatives for structural materials and structural systems. In general, it will provide a practical tool for engineers, analysts, and decision-makers to assess rapidly the LCC of any building based on its fundamental response quantities. The proposed method is verified through comparison with a more rigorous procedure applied to three different framed structures.

2. Framework for proposed LCC evaluation

The framework proposed in the current study is developed for preliminary estimation of LCC of any building at the early design stage, where there is no enough information available about the final finishing and nonstructural elements. In this case, the main input structural parameters such as stiffness, strength, and ductility are enough for the LCC estimation. In addition, this framework can help in the comparison among different structural system options for one building in the early structural design stage to decide which option would provide the minimum LCC for the building. Moreover, this framework can be used for the estimation of rough LCCs for an inventory of buildings or group of buildings that require LCC to be readily available without much computational effort to help designers and decision-makers. The proposed framework is different from the FEMA P-58 (2012) approach in such a way that it does not require details of the building components and element collapse fragilities.

2.1. The BRM (basic reference model)

The flow chart of the proposed LCC evaluation procedure is presented in Figure 1. The whole framework is developed using a basic reference model (BRM). As the framework may target an inventory of buildings or a group of buildings that require estimating their LCC readily, any building can be used to be a BRM. For example, a 3-story with 3- bay building having a total height of ten meters can be used as a BRM. Structural properties such as stiffness, strength, and ductility are obtained from the pushover curve of that building. These values will be used as a basis for calculating the LCC of the BRM.

The initial stiffness of a BRM, k, can be related to its natural period, T, and mass, m, by $k = [(2\pi/T)^2 m]$. In the current study, the value of the natural period of the BRM is set to be 1.0 sec. The strength ratio, SR, of the BRM can be defined as:

$$SR = V_y/mg \tag{1}$$

where V_y is the base-shear corresponding to a drift ratio of 1.0% of an elastic SDOF system, m is the mass of the system, and g is the gravity acceleration. The BRM ductility factor (μ) can be defined as:

$$\mu = y_m/y_y \tag{2}$$

where y_m is the maximum displacement that can be reached by the system, and y_y is the yield displacement of the system.

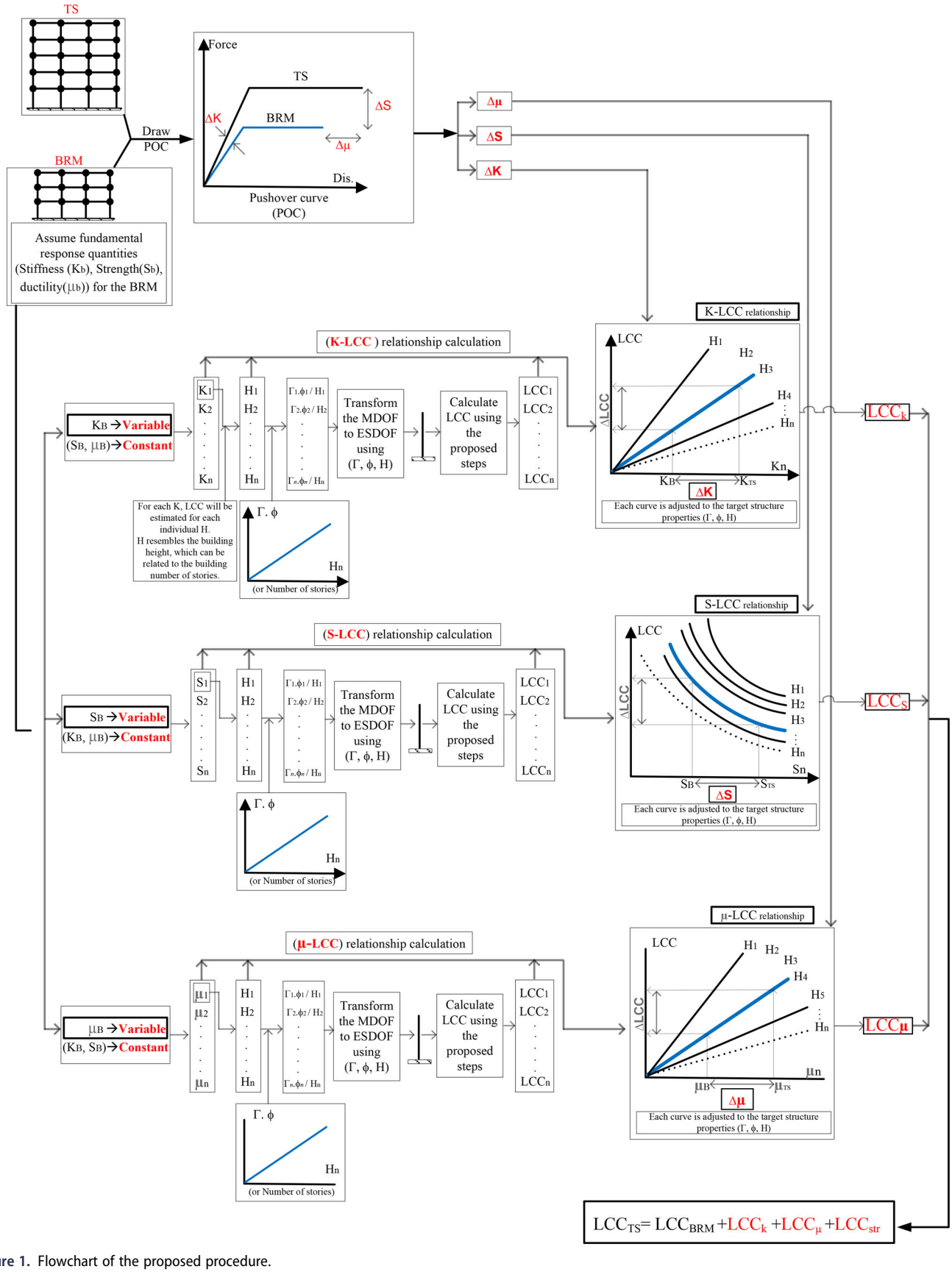

Figure 1. Flowchart of the proposed procedure.

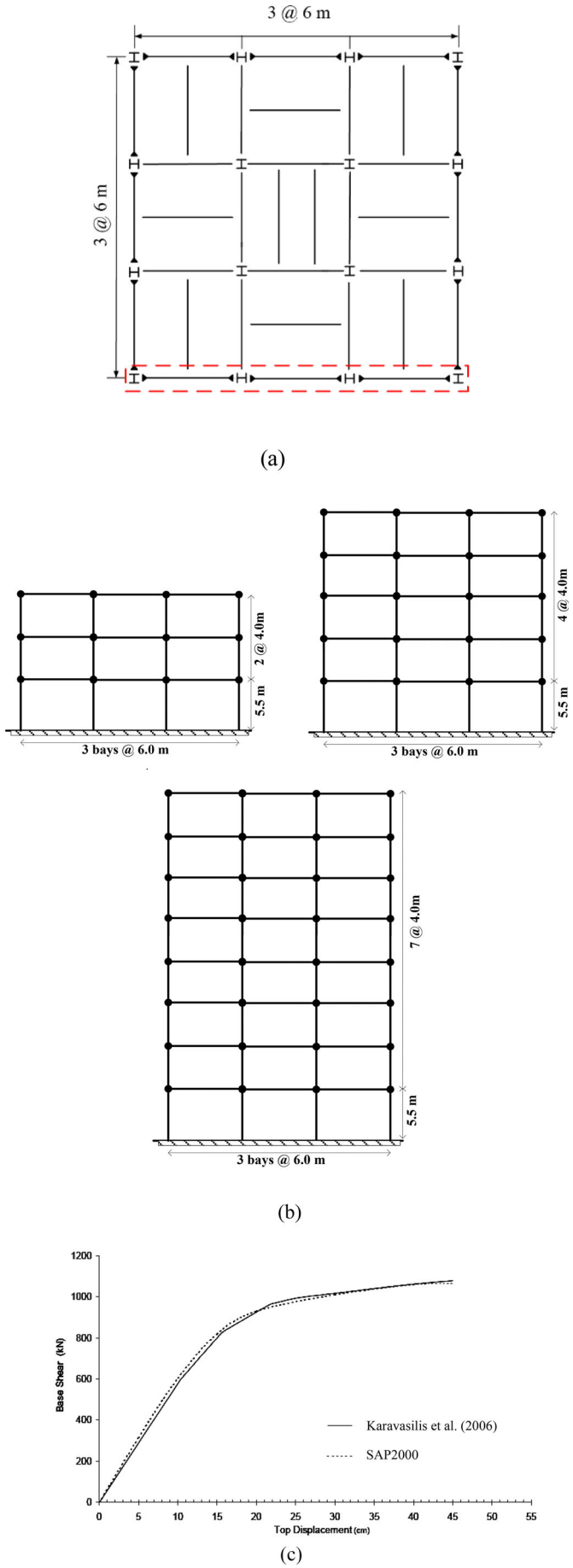

Figure 2. Prototype structures: (a) structural plan, (b) selected frames, (c) verification of the analysis modeling.

2.2. Relation between a BRM and a target structure

All the steps of estimating LCC are conducted on a BRM after it is transformed into an equivalent single degree of freedom (ESDOF) system using the hazard characteristics and the cost of exceeding the defined limit states of a target structure (TS). The LCC of a BRM is calculated and used as a reference for estimating the LCC of the TS. The pushover curves of the TS and BRM are drawn and the difference in stiffness, strength, and ductility are obtained. These differences is used as a basis to estimate the LCC of the TS. This will be achieved by establishing a relationship between the LCC and the main response quantities (i.e., stiffness, k, strength, S, and ductility, μ) of a BRM as shown in Figure 1. In this relationship, one response quantity (e.g., stiffness) will be changed while maintaining the other response quantities constant. Then a relationship between the LCC and this response quantity will be established for different story numbers or different building heights (H). The current study is focusing on low to mid-rise buildings. The LCC of a BRM will be estimated and then adjusted by the properties of a TS such as height, participation factor, etc. After that, the difference between the BRM and the TS in stiffness, strength, and ductility will be used to calculate the corresponding difference in LCC between the two systems.

The details of the transformation into ESDOF system can be found elsewhere (Saiidi & Sozen, 1981; Fajfar & Fischinger, 1988). The ESDOF simplification is based on the assumption that the seismic response of a structure is dominated by a single mode and that the shape of this mode remains invariant throughout the analysis. This enables us to relate the response of the multi-degree of freedom (MDOF) structure with the response of an equivalent single degree of freedom (SDOF) system. Pushover analysis is used to obtain the capacity curve of the structure. The lateral-force pattern is proportional to the product of masses and fundamental mode shape. The structure capacity curve is idealized to a bilinear force-displacement relationship, which is established in such a way that the areas under the idealized and the capacity curves are equal.

The following equation is used for obtaining the maximum inter-story drift ratios (MIDR) of any structure from the inelastic deformation of the ESDOF system, $s_{SDOF(inel)}$, (assuming uniform inter-story drift ratios):

$$MIDR_{MDOF} = s_{SDOF(inel)} \frac{\Gamma.\varphi_r}{H} \tag{3}$$

where Γ is the modal participation factor; φ_r is the modal amplitude at the roof of the fundamental mode shape; and H is the height of the structure. The following equation is used to calculate Γ :

$$\Gamma = \sum_{1}^{n} m_i \varphi_i / \sum_{1}^{n} m_i \varphi_i^2 \tag{4}$$

where m_i and φ_i are the mass and modal amplitude assigned to the DOF i of the fundamental mode shape normalized to have a modal mass equal to unity. This implies that:

Table 1. Cross-sections of the model structures (all sections are wide flange).

		Columns (left to right)				Beam (left to right)		
Model	Story/Bay	A	B	C	D	1	2	3
3	1	14 × 43	12 × 40	10 × 40	14 × 43	10 × 45	10 × 45	10 × 45
	2	12 × 26	12 × 30	14 × 30	12 × 26	10 × 39	10 × 39	10 × 39
	3	10 × 26	6 × 15	6 × 15	10 × 26	10 × 39	10 × 39	10 × 39
5	1	14 × 53	12 × 58	12 × 58	14 × 53	10 × 60	10 × 60	10 × 60
	2	14 × 38	14 × 48	14 × 48	14 × 38	10 × 60	10 × 60	10 × 60
	3	8 × 35	8 × 40	8 × 40	8 × 35	10 × 60	10 × 49	10 × 60
	4	8 × 28	8 × 31	8 × 31	8 × 28	8 × 58	8 × 58	8 × 58
	5	8 × 31	8 × 21	8 × 21	8 × 31	8 × 48	8 × 48	8 × 48
8	1	12 × 65	12 × 72	12 × 72	12 × 65	12 × 65	12 × 65	12 × 65
	2	10 × 45	12 × 58	12 × 58	10 × 45	10 × 60	10 × 60	10 × 60
	3	8 × 48	8 × 58	8 × 58	8 × 48	10 × 60	10 × 60	10 × 60
	4	8 × 40	8 × 58	8 × 58	8 × 40	8 × 67	8 × 67	8 × 67
	5	8 × 40	8 × 58	8 × 58	8 × 40	8 × 67	8 × 67	8 × 67
	6	8 × 31	8 × 40	8 × 40	8 × 31	8 × 58	8 × 58	8 × 58
	7	8 × 28	8 × 28	8 × 28	8 × 28	8 × 48	8 × 48	8 × 48
	8	8 × 31	8 × 18	8 × 18	8 × 31	8 × 48	8 × 48	8 × 48

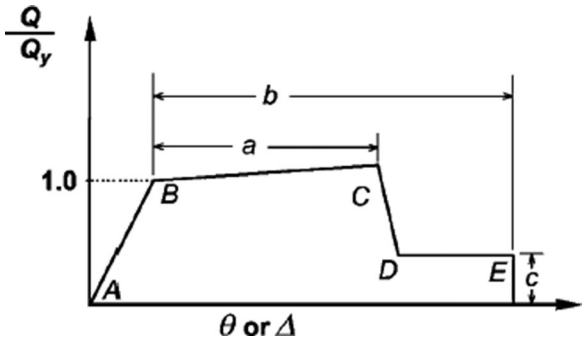

Figure 3. Generalized force-deformation relationship for beams and columns.

$$\sum_{1}^{n} m_i \varphi_i = 1 \tag{5}$$

To account for the probabilistic relationship between the analysis results of an ESDOF and MDOF systems, the MIDR obtained from the ESDOF system is multiplied by 1.13 as recommended by Jeong and Elnashai (2007). As there is no irregularity in mass or stiffness in the structures under consideration, the average inter-story drift ratio will be adequate to be representative of the structure response. It is worth mentioning that the CSM permits the direct determination of the inelastic deformation of the ESDOF, $s_{SDOF(inel)}$, using diagrams similar to the standard response spectrum and variation curves for the equivalent vibration period that depends on the elastic period and the ratio between the yield and elastic strength of the system.

2.3. Design and modeling of the case study structures

In the proposed framework, a set of steel special moment-resisting frame prototype buildings, three to ten-story high, are designed based on AISC 360 (2016). The first and the typical story heights are 5.5 m and 4.0 m, respectively, and the bay width is 6.0 m. The plan and elevation of the exterior frame for three examples of the prototype structures are shown in Figure 2. Based on ASCE 7 (2016), the design live and dead loads are taken as 2.5 kN/m^2 and 4.1 kN/m^2, respectively. Wide flange sections are used for all beams and columns as shown in Table 1. The natural frequencies of the three, five, and eight-story frame examples shown in the figure are 0.66, 0.48, and 0.32 Hz, respectively.

To verify the accuracy of the non-linear modeling and analysis using the SAP2000 software, a three-bay six-story steel frame adopted from Karavasilis, Bazeos, and Beskos (2006) study is investigated. The details of the steel frame can be found in the same study. The structure is modeled in SAP2000 software and the results of the non-linear static pushover curve are compared with those obtained from the same reference. The pushover curves are depicted in Figure 2(c) for verification. As can be observed in the figure, the two pushover curves are almost identical. ASCE/SEI 41, 41 (2013) recommendations are used for defining plastic hinges, which will be introduced at the ends of the beams and columns in the nonlinear time history-response analysis (NLTHA) of the model structures using SAP2000.,2000 (2018).

Figure 3 displays the generalized force-deformation relationship of the beams and columns used in the analysis. In this figure, the vertical axis represents the ratio between the applied action (force or moment, Q) and the yield value, Q_y, and the horizontal axis represents the deformation (rotation angle, θ, or displacement, Δ). The parameters a and b refer to the deformation portions that occur after yield, or plastic deformation. The parameter c is the reduced resistance after the sudden reduction from C to D. Parameters a, b, and c are defined numerically in ASCE/SEI 41, 41 (2013). These parameters are calculated for each section automatically by the analysis software. The IO (immediate occupancy), LS (life safety), and CP (collapse prevention) limit states are based on the performance criteria defined in ASCE/SEI 41, 41 (2013). A modal damping ratio of 2% of the critical damping is used in the NLTHA.

2.4. Seismic hazards and earthquake ground motions

Generally three different methods are used for the correspondence between hazard levels and ground motions (Gencturk & Elnashai, 2012). The first uses natural records without any modifications. The second uses scaling of the records' PGA to match that of the hazard levels. The third

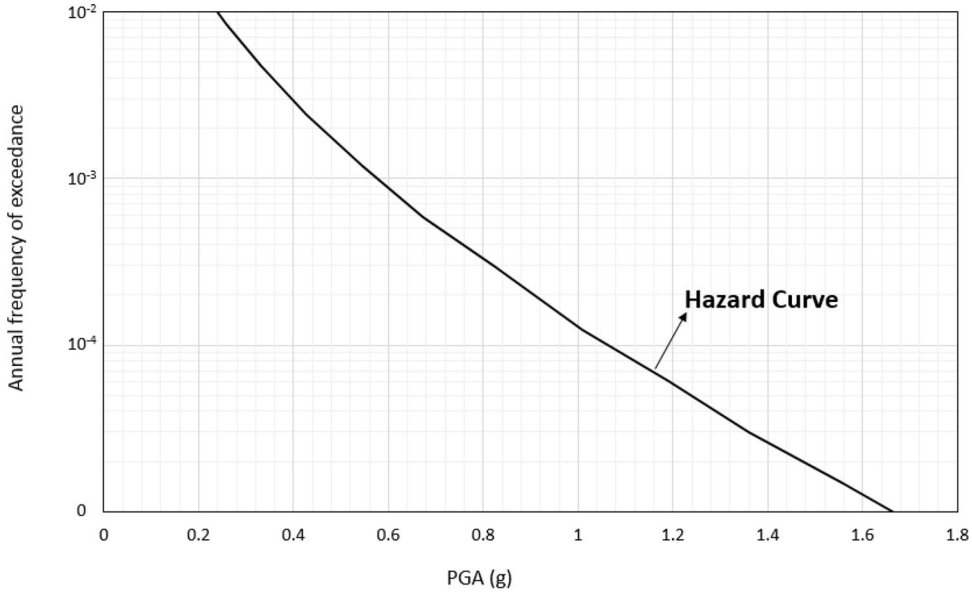

(a) Seismic hazard curve of Los Angeles

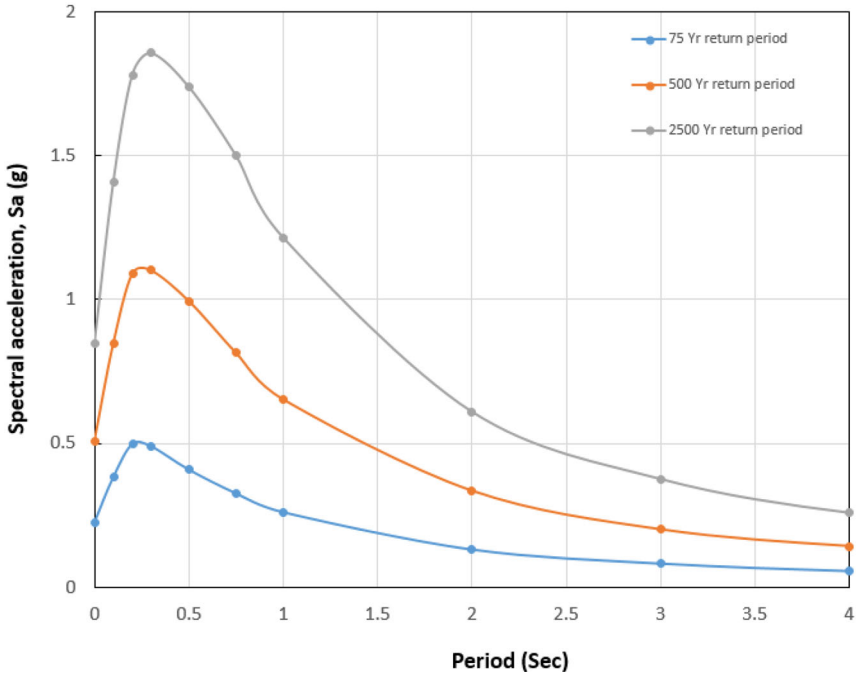

Figure 4. Seismic hazard curves and uniform hazard spectra used in the analysis (Noureldin et al., 2019).

uses spectrum matching where every record spectrum matches the hazard level spectrum. The first two methods are recommended for LCC assessment. In the current study, PGA scaling method is used. The site-specific hazard curve of a county in Los Angeles with soil type D (S_{DS}=1.46 and S_{D1}=0.737) is constructed as shown in Figure 4(a) based on the information provided by the USGS (2017). 75, 500, and 2500 years return periods uniform hazard spectra of this site are shown in Figure 4(b). These return periods are linked with immediate occupancy (IO), life safety (LS), and collapse prevention (CP) limit states, respectively (ASCE/SEI 41, 41 (2013); Fragiadakis, Lagaros, and Papadrakakis (2006); Gencturk (2013)).

Table 2 presents three sets of ground motions extracted from the Pacific Earthquake Engineering Research NGA database. Since the main focus of the current study is to propose a simplified procedure for LCC estimation, more variability is introduced in the input ground motions to guarantee the effectiveness of the procedure under different circumstances. In this study two different mechanisms are used in the selection criteria, which are strike-slip and reverse mechanisms. The magnitudes of the earthquake records range from 6.0 to 7.5, and the shear wave velocity ranges from 160 m/s to 530 m/s. The maximum distance to the rupture plane of 40.0 km is used. Pulse-like records are not considered in the selection criterion. The ground motions are scaled with

Table 2. Selected ground motions for different hazard levels*.

Return Period	NGA #	PGA (g)	Earthquake Event	Year	Station	Mag.	Vs (m/sec)	Distance (km)	Mechanism
75 YRP	15	0.24	Kern County	1966	Taft Lincoln School	7.36	256.82	38.89	Reverse
	20	0.26	Northern California	1954	Ferndale City Hall	6.5	219.31	27.02	strike slip
	68	0.31	San Fernando	1971	LA - Hollywood Stor FF	6.61	316.46	22.77	Reverse
	138	0.14	Tabas Iran	1978	Boshrooyeh	7.35	324.57	28.79	Reverse
	161	0.28	Imperial Valley	1979	Brawley Airport	6.53	208.71	10.42	strike slip
	163	0.15	Imperial Valley	1979	Calipatria Fire Station	6.53	205.78	24.6	strike slip
	164	0.23	Imperial Valley	1979	Cerro Prieto"	6.53	202.85	15.19	strike slip
	172	0.20	Imperial Valley	1979	El Centro Array #1	6.53	237.33	21.68	strike slip
	175	0.19	Imperial Valley	1979	El Centro Array #12	6.53	196.88	17.94	strike slip
	176	0.18	Imperial Valley	1979	El Centro Array #13	6.53	249.92	21.98	strike slip
500 YRP	6	0.35	Imperial Valley	1940	El Centro Array #9	6.95	213.44	6.09	strike slip
	158	0.42	Imperial Valley	1979	Aeropuerto Mexicali	6.53	259.86	0.34	strike slip
	161	0.28	Imperial Valley	1979	Brawley Airport	6.53	208.71	10.42	strike slip
	165	0.37	Imperial Valley	1979	Chihuahua	6.53	242.05	7.29	strike slip
	169	0.43	Imperial Valley	1979	Delta	6.53	242.05	22.03	strike slip
	170	0.32	Imperial Valley	1979	EC County Center FF	6.53	192.05	7.31	strike slip
	171	0.44	Imperial Valley	1979	El Centro - Meloland Geot	6.53	264.57	0.07	strike slip
	173	0.29	Imperial Valley	1979	El Centro Array #10	6.53	471.53	8.6	strike slip
	174	0.53	Imperial Valley	1979	El Centro Array #11	6.53	196.25	12.56	strike slip
	178	0.35	Imperial Valley	1979	El Centro Array #3	6.53	162.94	12.85	strike slip
2500 YRP	6	0.35	Imperial Valley	1940	El Centro Array #9	6.95	213.44	6.09	strike slip
	30	0.59	Parkfield	1966	Cholame - Shandon	6.19	289.56	9.58	strike slip
	31	0.38	Parkfield	1952	Cholame - Shandon	6.19	385.43	12.9	strike slip
	33	0.46	Parkfield	1966	Temblor pre-1969	6.19	527.92	15.96	strike slip
	57	0.43	San Fernando	1971	Castaic - Old Ridge Route	6.61	450.28	22.63	Reverse
	95	0.50	Managua Nicar	1972	Managua_ ESSO	6.24	288.77	4.06	strike slip
	125	0.48	Friuli Italy	1976	Tolmezzo	6.5	505.23	15.82	Reverse
	126	1.22	Gazli USSR	1976	Karakyr	6.8	259.59	5.46	Reverse
	139	0.53	Tabas Iran	1978	Dayhook	7.35	471.53	13.94	Reverse
	158	0.42	Imperial Valley	1979	Aeropuerto Mexicali	6.53	259.86	0.34	strike slip

*All records are fault normal components.

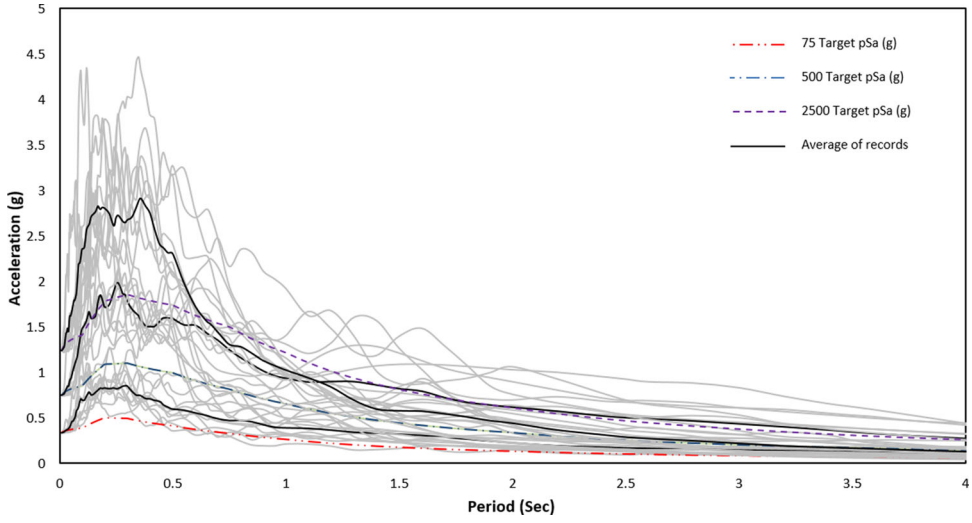

Figure 5. Response spectra of ground motions and their geometric mean scaled to PGA of UHS with 75, 500 and 2500 year return periods (Noureldin et al., 2019).

respect to the peak ground acceleration of each uniform response spectrum as shown in Figure 5. To avoid any distortion of the ground motion characteristics, the scaling factor should be limited to certain levels such as 10.0 (Hancock, Bommer, & Stafford, 2008) or 4.0 (Iervolino & Cornell, 2005). The latter scale factor is used in the current study.

2.5. The steps for calculating the LCC of the BRM

1. Obtain the hazard curve of the location of the structure. Select three different hazard levels with various recurrence periods such as 75, 500, and 2500 years corresponding to three different limit states; IO, LS, and CP. The hazard curve is almost linear on a log-log plot in the region of interest and can be approximated by the following exponential form (Cornell, Jalayer, Hamburger, & Foutch, 2002):

$$H(s_a) = P[S_a \geq s_a] = k_o s_a^{-k} \tag{6}$$

where s_a is the elastic spectral acceleration (a measure of ground motion intensity); $H(s_a)$ is the hazard function of spectral acceleration, the annual frequency that intensity S_a at a site will equal or exceed s_a; k_o and k are the coefficients for linear regression of hazard $H(s_a)$

on intensity S_a in the proximity of the limit-state probability (region of interest) in logarithmic space. At small values, the frequency of exceedance is almost the same as the probability of exceedance. These coefficients control the slope and the degree of nonlinearity, respectively, of the hazard curve (Aslani & Miranda, 2005). The hazard curve may not always be linear in the log-log space. In this case, the equation of the hazard should be used and the curvature of the hazard curve should be considered. The hazard curve can be constructed based on the PGA or the natural period of the structure under investigation.

2. For the BRM, calculate the corresponding inelastic spectral displacement and acceleration using any simple method, such as the capacity spectrum method (ATC 40, 40, 1996), as shown in Figure 1. This will be conducted for each hazard demand spectrum.
3. Linear regression of drift demand S_d on intensity S_a in a logarithmic space is obtained using the following equation:

$$S_d = a(S_a)^b \tag{7}$$

where a and b are the regression coefficients that control the slope and degree of nonlinearity, respectively (Aslani & Miranda, 2005). Previous studies such as Cornell et al. (2002) and Luco and Cornell (1998, 2000) suggest $b = 1.0$ for moment frames.

4. After defining the limit state, the capacity spectral acceleration corresponding to each limit state, $S_a^{\hat{c}}$, is calculated from the previous step. After that, $H\left(S_a^{\hat{c}}\right)$ can be computed using Equation (6).
5. The dispersion measure in demand $\beta_{D|s_a}$ for each limit state can be obtained using two alternatives. The first one is based on generating the mean-plus-one-standard deviation response spectrum using amplification factors recommended by Newmark and Hall (1982) and illustrated by Chopra (2007). From both the elastic mean and mean-plus-one-standard deviation response spectra, the inelastic responses of the SDOF system can be calculated. This is the method used in the current study. The difference between the two responses indicates the standard deviation in demand, which is $\beta_{D|Sa}$. The second alternative is based on the reasonable assumption of $\beta_{D|s_a}$ as suggested in the literature for each limit state. For example, Gencturk (2013) assumed $\beta_{D|s_a}$ as 0.3, 0.4, and 0.5 for IO, LS, and CP limit states, respectively.
6. The structural capacity uncertainty, which is represented by the dispersion capacity factor, β_C, is assumed to be 0.35 based on previous researches (Gencturk, 2013).
7. The limit state probability, P_{Ls}, can be obtained by Cornell et al. (2002):

$$P_{Ls} = H\left(S_a^{\hat{c}}\right) \exp\left[\frac{1}{2}\frac{k^2}{b^2}\left(\beta_{Ds_a}^2 + \beta_C^2\right)\right] \tag{8}$$

where all parameters are defined previously.

8. The LCC of a structure can be calculated as follows (Wen & Kang, 2001):

$$\begin{aligned} E[C_{Lc}] &= C_o + \int_0^L E[C_{SD}]\left(\frac{1}{1+\lambda}\right)^t dt \\ &= C_o + \alpha L\ E[C_{SD}] \end{aligned} \tag{9}$$

where C_o is the initial construction cost, L is the service life of the structure, λ is the annual discount rate (assumed to be 0.03), and $E[C_{SD}]$ is the annual expected seismic damage cost, which is governed by a Poisson process and does not depend on time; and the structure is considered to be restored to its as-built condition after each hazard (Gencturk, 2013). The parameters α, q and $E[C_{SD}]$ can be formulated as:

$$\alpha = \left[1 - \exp(-qL)/qL\right] \tag{10}$$

$$q = \ln(1+\lambda) \tag{11}$$

$$E[C_{SD}] = \sum_{i=1}^{N} C_i.\ P_i \tag{12}$$

where N is the total number of limit-states considered, P_i is the total probability that the structure is in the i^{th} limit state throughout its lifetime, and C_i is the corresponding cost including the cost of damage and its repair. In accordance with the definition of seismic hazard, three structural limit states are used (i.e., N is equal to three) such as IO, LS, and CP, and C_i is assumed to be 30, 70 and 100%, respectively, of the initial cost of the structure taking previous studies into consideration (e.g., Gencturk and Elnashai (2012); Lagaros, Fotis, and Krikos (2006); Fragiadakis et al. (2006)). P_i is given by

$$P_i = P(\Delta_D > \Delta_{C,i}) - P(\Delta_D > \Delta_{C,i+1}) \tag{13}$$

where Δ_D is the earthquake demand and $\Delta_{C,i}$ is the structural capacity, usually represented in terms of drift ratio, defining the i^{th} limit state. The probability of demand is greater than capacity, $\Delta_D > \Delta_{C,i}$, is evaluated as discussed in the previous steps. The repair costs used in the current study are based on previous studies as mentioned; however they can be changed based on factors such as type of buildings, seismic design category, importance factor, etc.
9. Draw the pushover curve of the TS and obtain the difference in stiffness, strength, and ductility between the TS and the BRM as shown in Figure 1. Pushover curves are constructed using a lateral load pattern that is proportional to the first mode amplitudes multiplied by the masses.

Steps 1–8 will be followed to obtain the LCC of the BRM having the same stiffness of the TS without changing the strength or ductility. The difference in LCC between the BRM and BRM-stiffness-adjusted is LCC_k. Similarly, one can obtain the LCC_{str} for BRM-strength-adjusted, and LCC_μ for BRM-ductility-adjusted. The final LCC of the TS can be estimated as:

$$LCC_{TS} = LCC_{BRM} + \Delta LCC_k + \Delta LCC_{str} + \Delta LCC_\mu \tag{14}$$

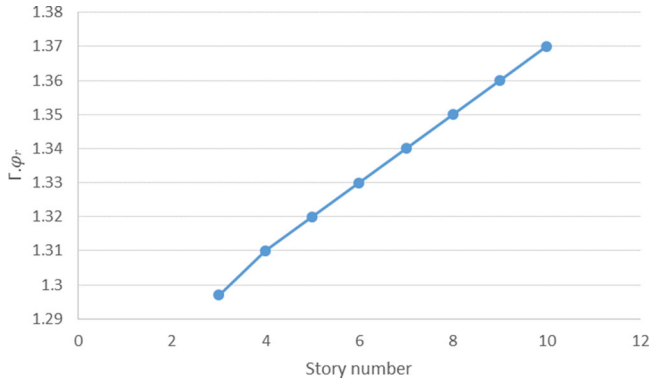

Figure 6. Relationship between the number of stories and the conversion factor ($\Gamma.\varphi_r$) keeping the mass, the height of the story, and the number of bays the same.

The LCC_{BRM} term in the above equation is adjusted to the TS characteristics, i.e., the initial cost of the TS is included in this term. This means that this term will be different for each building case. In the case of retrofitting an existing structure, the additional cost of the retrofit should be included in the initial cost. More details about stiffness, strength, and ductility adjusted-BRM are given in the next section.

The proposed method takes into account the limit state definition as stated in the first step of the procedure. Any change in this definition will be reflected through P_i, which is the total probability that the structure is in the i^{th} limit state throughout its lifetime (Equation 12). Moreover, any number of limit states can be considered in the proposed procedure. This implies that the proposed procedure is versatile enough to account for any variability in the limit state definitions.

3. Relationship between LCC and the fundamental response quantities of structures

In this section, the relationship between LCC and the structure fundamental response quantities is investigated. Using a set of prototype structures, graphs that relate LCC with the stiffness, strength, and ductility will be established.

3.1. Stiffness-LCC relationship

To obtain the relationship between LCC and the natural period T of a structure, LCC is calculated using the characteristics of each building (i.e., Γ, H, and φ_r) for different T values as shown in Figure 1. In order to simplify the transformation to ESDOF system, a set of moment-resisting frame structures have been investigated to obtain the relationship between the number of stories and the conversion factor ($\Gamma.\varphi_r$). Figure 6 presents the relationship between the number of stories and the conversion factor ($\Gamma.\varphi_r$) maintaining the mass, the height of the story, and the number of bays the same as those of the case study structures. Having all other variables fixed at the best estimate, LCC can be calculated for the corresponding T. The ductility and the strength of the structure are fixed at the BRM values. This means that the only variable is the stiffness, which is represented by T. Then, a T-LCC relationship can be drawn showing a different number of stories for each curve (Figure 7). In this figure, at any single period, the LCC is calculated for a different number of stories as shown using the steps outlined in section 2.5. As shown in the figure, the LCC increases with the increase in T. This means that the decrease in stiffness for the same building results in increasing its LCC.

The idea in obtaining inelastic displacement is that if an unlimited elastic behavior for each structure is assumed, the straight line represented by the period of the structure on the ADRS (acceleration-displacement response spectra) format will intersect with each of the three demand curves at the corresponding performance point. This applies to the case in which the equal displacement rule is effective. The difference in the spectral displacements between the BRM and the target structure will lead to a corresponding difference in LCC due to the difference in stiffness.

3.2. Strength-LCC relationship

In order to obtain an LCC-strength relationship shown in Figure 1, it is necessary to relate the strength to one of the variables in the procedure of calculating the LCC. The strength of a structure can be determined through the known stiffness and the limit state of the Immediate Occupancy (IO), which corresponds to the end of the linear phase of the pushover curve. The intersection between the vertical line representing the IO limit state and the radial line originating from the origin (the elastic portion of the pushover curve) indicates the strength of the structure.

The BRM is adjusted based on the characteristics of the target structure (TS) (i.e., Γ, height), then the corresponding LCC is computed setting the IO limit state to two different values. The first value of the IO is 1.0% of the story height, and the corresponding LCC is $LCC_{adj,IO=1\%}$. The other value is the displacement obtained from the pushover curve of the target structure, and the corresponding LCC is denoted as $LCC_{adj,IO=TS}$. The difference between the two LCCs is due to the difference in strength between the BRM and TS, which is $LCC_{str} = LCC_{adj,IO=TS} - LCC_{adj,IO=1\%}$.

Figure 8 depicts the relationship between the strength ratio and the LCC of structures with a different number of stories. In this figure, the LCC is calculated for a different number of stories using the steps outlined in section 2.5 knowing the stiffness of the structure and the IO limit state. As shown in the figure, the LCC decreases with the increase in the strength ratio. In addition, the rate of decrease in LCC is larger for smaller strength ratios for the same building.

3.3. Ductility -LCC relationship

In order to establish an LCC-ductility relationship, we need to calculate $S_{din2500}$ (inelastic displacement for the 2500-year return period spectrum) corresponding to the natural period of BRM, i.e., $T = 1.0$ sec, and that of the target structure obtained from the modal analysis, i.e., T_{TS}. The following equations can be used in this process:

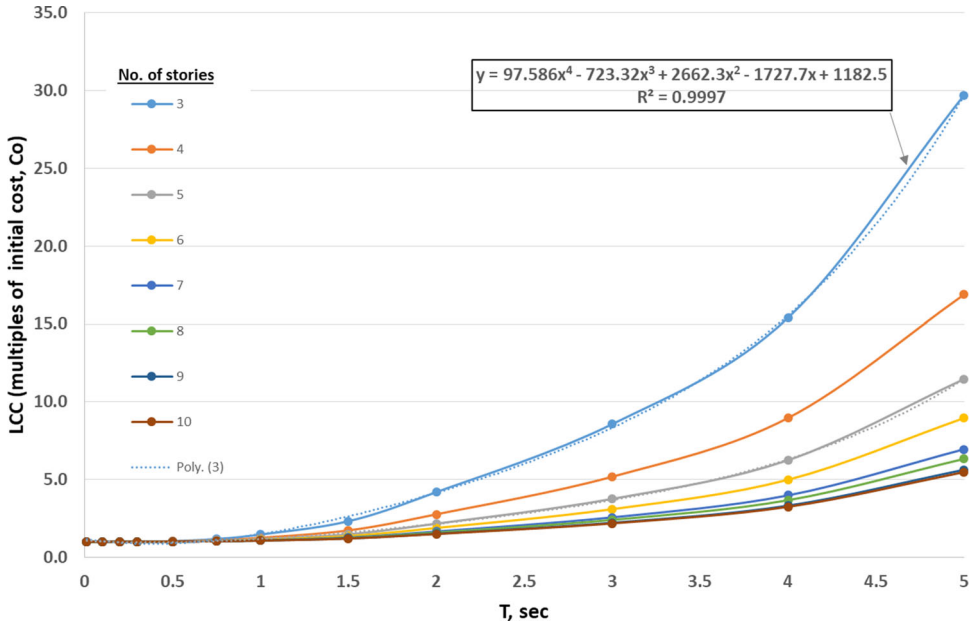

Figure 7. Relationship between the fundamental period and the LCC for structures having a different number of stories.

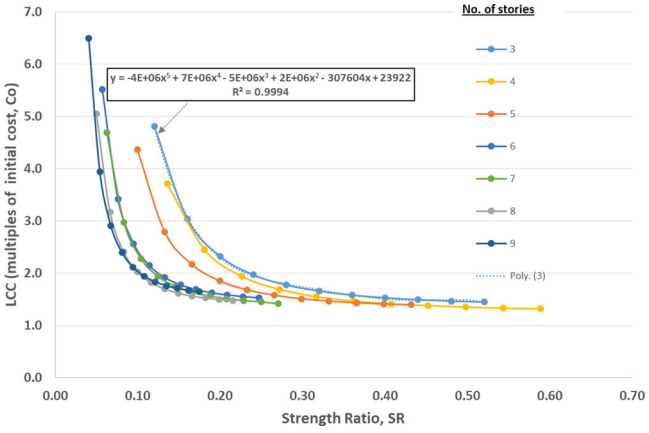

Figure 8. Relationship between the strength ratio and the LCC for a different number of stories.

$$S_{de} = \frac{T^2}{4\pi^2} S_{ae} \tag{15}$$

where S_{ae} and S_{de} are the values of the elastic pseudo-acceleration and displacement, respectively:

$$S_d = \frac{\mu}{R_\mu} S_{de} \tag{16}$$

where μ is the ductility factor defined as the ratio between the maximum system displacement and the yield displacement, and R_μ is the reduction factor associated with the hysteretic energy dissipation of the ductile structures. In the current study, μ and R_μ are related by the following bilinear relation (Newmark & Hall, 1982):

$$R_\mu = (\mu - 1)\frac{T}{T_c} + 1 \quad T < T_c \tag{17}$$

$$R_\mu = \mu \quad T \geq T_c \tag{18}$$

where Tc is the characteristic period of the ground motion, which is defined as the transition period where the constant acceleration segment of the response spectrum (the short-period range) passes through the constant velocity segment of the spectrum (the medium-period range). In the current study, Tc is 0.107 second. This bilinear $R\mu$ - μ relation suggests that in the medium- and long-period ranges, the equal displacement rule applies. That implies that the displacement of the inelastic SDOF system is equal to the displacement of the corresponding elastic SDOF system with the same period.

After obtaining $S_{din2500BRM}$ and $S_{din2500TS}$, the LCC can be calculated for the BRM after being adjusted to the height and the participation factor of the target structure. The difference between the two values of the LCC is considered the effect of the difference in the ductility factor between the BRM and the TS. It is worthwhile to mention here that the ductility demand is used rather than the ductility supply in the proposed procedure. This is because the ultimate displacement that will be used in the proposed LCC calculation is related to the ductility demand. Nevertheless, the ductility supply is included in determining the collapse limit state (Jeong & Elnashai, 2007). ASCE/SEI-41 (2013) recommends the collapse-prevention (CP) limit-state to be the transient drift sufficient to cause extensive nonstructural damage (assumed 4.0% in the current study). Figure 9 shows the relationship between the ductility ratio and the LCC for a different number of stories. In this figure, for any ductility ratio, the LCC is calculated using the steps outlined in section 2.5 for a different number of stories. As shown in the figure, the LCC increases with the increase in the ductility ratio almost in a linear fashion.

Figure 10 displays a schematic diagram of the relationship between the main system response quantities (stiffness, strength, and ductility) and the LCC. The relationship between the LCC and any response quantity can be established through drawing graphs (as in Figures 7–9) or through knowing the equation that governs this relation as indicated in the figures for one building as an example.

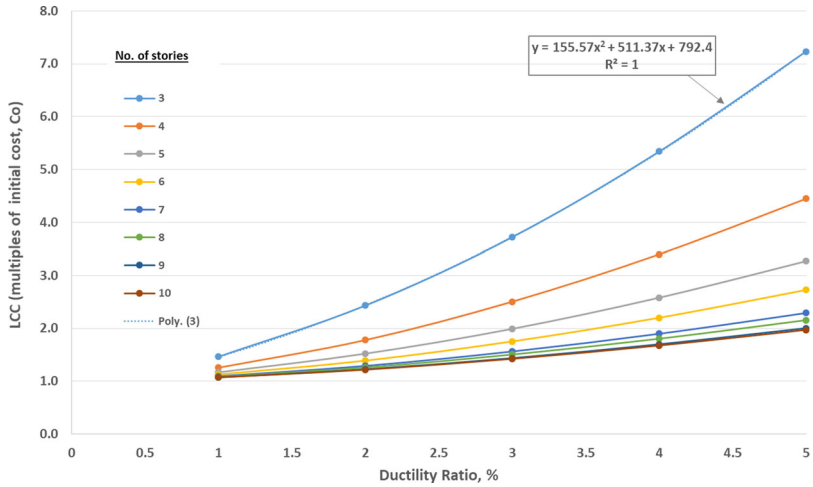

Figure 9. Relationship between the ductility ratio and the LCC for a different number of stories.

Based on that, the addition of the LCC suggested by Equation (14) can be justified.

4. Verification of the proposed framework

In order to validate the proposed LCC methodology, a comparison is made with the results obtained from a more rigorous method referred to as the 'reference method' for the 3-, 5-, and 8-story frames. In the reference method, most of the simplifications made in the proposed procedure are avoided. The whole structure, i.e., the MDOF system, is used instead of the ESDOF system, and the full fragility curves are constructed to capture accurately the capacity spectral acceleration for each limit state. In addition, for each hazard, thirty time-history records are used to represent accurately the dispersion in demand associated with each hazard level. Each record is scaled to the spectral acceleration of the structure with increasing intensity until dynamic instability occurs.

The fragility curves of the 5-story TS model are shown in Figure 11 as an example, and Table 3 shows the parameters used in the LCC estimation. The LCC estimations obtained using the proposed and the reference methods are compared in Figure 12. As shown in the figure, the LCCs estimated by the proposed method are slightly different compared to those of the reference method. In general, the proposed method provides an upper bound for the LCC estimation for all of the selected example structures.

In the 3-story model, the LCCs obtained from the reference and the proposed methods, as a percentage of the initial cost, are 2.069 and 2.118, respectively, which differ in about 2.4%. On the other hand, the LCCs obtained for the 5-story model are 1.588 and 1.778, respectively, which differ in about 11.9%. In the case of the 8-story model, the LCCs obtained are 2.024 and 2.143, respectively, which differ in about 5.9%. The relatively large discrepancy in the 5-story model can be attributed to the ESDOF system approximation, which seems to be insufficient to capture accurately the actual behavior of the structure, especially in the structural response with large deformation.

Table 4 lists the values used for calculating the difference in LCC due to the difference in stiffness between the BRM and the TS. It can be observed that an increase in the fundamental period of the structure, which means a decrease in the stiffness, causes an increase in the LCC. This is true because the probability of exceeding the limit states is higher in the structures with small stiffness compared to the structures with large stiffness. The differences in LCC due to the difference in the stiffness of the BRM and the TS are found to be 0.858, 0.995, and 1.557 of the initial cost, respectively, for the 3, 5, and 8-story structures.

Table 5 presents the values used for calculating the difference in LCC due to the difference in strength between the BRM and the TS. As shown in the table, the increase in the strength ratio of the structure results in a decrease in the LCC. The strength ratios of the BRM after being adjusted to the TS are 0.2, 0.102, and 0.034, respectively, for the 3, 5, and 8-story structures. The strength ratios of the TS are 0.41, 0.34, and 0.2, respectively, for the 3, 5, and 8-story structures. The difference in strength ratios of the BRM and the TS results in a decrease of the LCC by 0.708, 0.731, and 0.818 of the initial cost, respectively for the 3, 5, and 8-story structures. The results indicate that the large difference in strength ratios between the BRM and the TS, as in the 8-story case, may not have a significant impact on LCC. This can be attributed primarily to the effect of the low stiffness, which offsets the impact of the large increase in strength.

Table 6 shows the values used for calculating the difference in LCC due to the difference in the ductility ratio between the BRM and the TS. The table shows that the increase in the ductility factor causes an increase in LCC. The ductility factor increases from 2.2 for the BRM to 3.53, 4.50, and 6.22 for the 3, 5, and 8-story structures, respectively. This increase in the ductility factor results in an increase of the LCC, as a fraction of C_o, by 0.505, 0.345, and 0.366 for the same structures, respectively. The results indicate that the large difference in ductility ratio between the BRM and the TS, as in the 8-story case, may not have a significant effect on LCC. This can be attributed primarily to the effect of the stiffness and the strength, which offset partially the impact of the large increase in ductility.

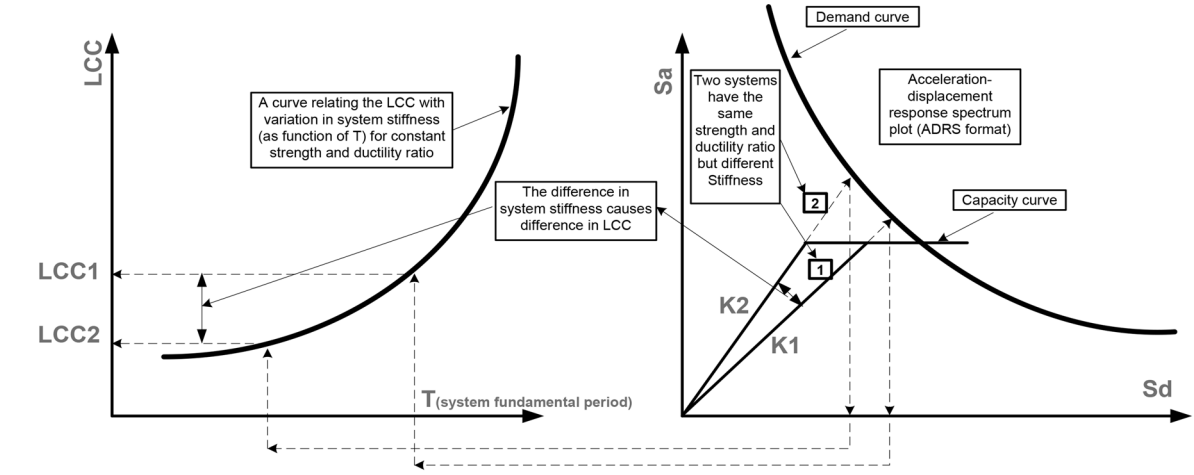

(a)

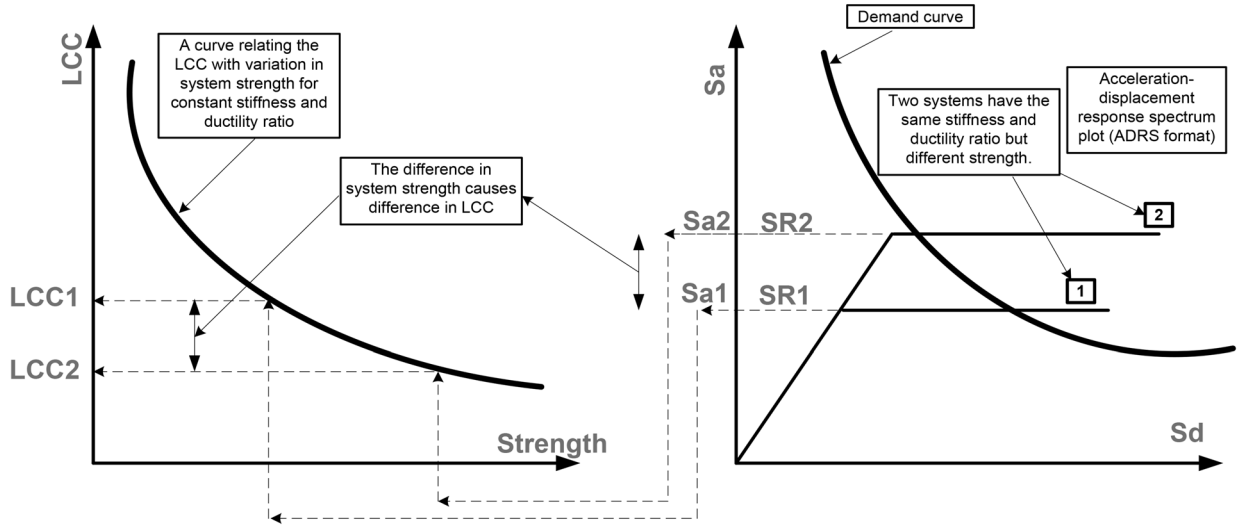

(b)

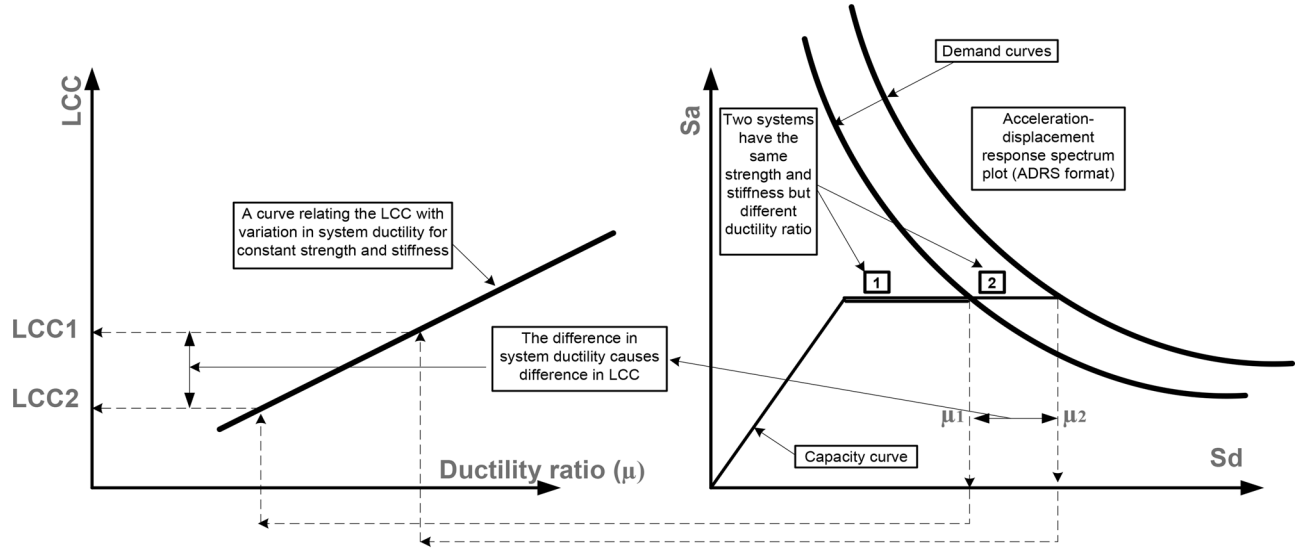

(c)

Figure 10. A schematic diagram for the relationship between the LCC and the system: (a) stiffness, (b) strength and (c) ductility.

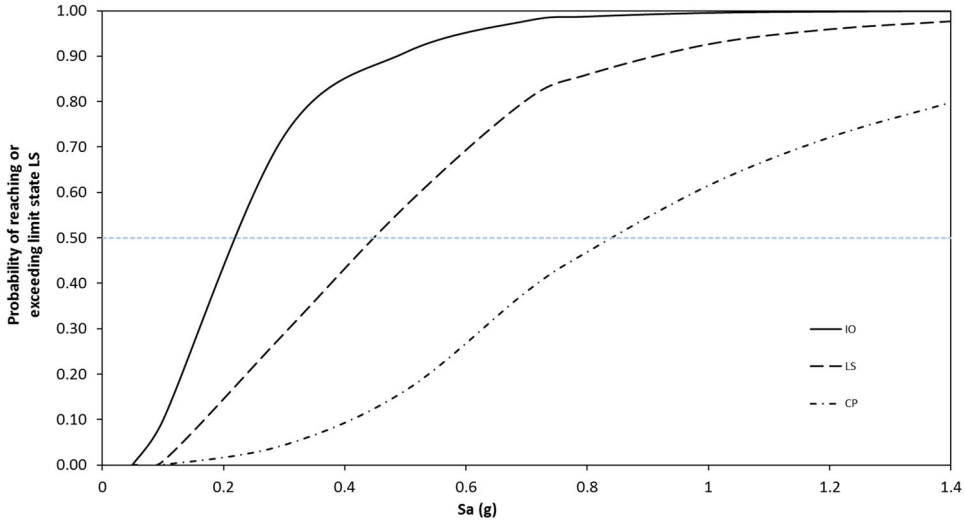

Figure 11. Fragility curves of the 5-story structure using the rigorous method.

Table 3. Parameters used in LCC estimation of the original 5-story structure.

Parameter	Value		
Limit state	IO	LS	CP
S_A^C (g)	0.22	0.49	0.78
$\beta_{D\|Sa}$	0.60	0.57	0.57
H (S_a)	0.01286	0.00180	0.00031
k_o		0.0002	
k		2.75	
b		1.0	
β_c		0.3	
$P(L_S \|_{Sa})$ %	7.05	0.86	0.15
P_i (%)	6.19	0.71	0.15
Limit state exceedance cost	0.3 C_o	0.7 C_o	C_o
(C_o) ($)		688,500	
LCC ($)		1,093,482	

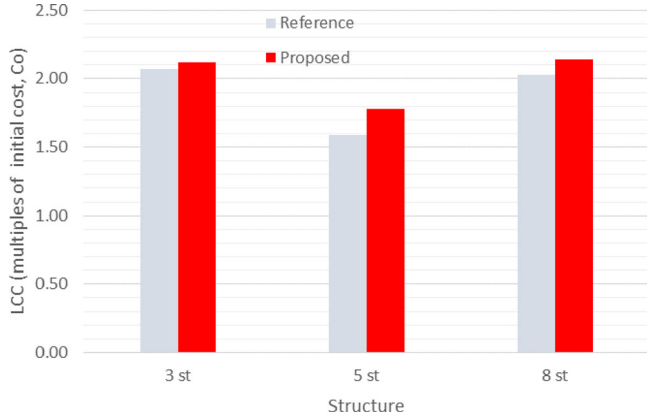

Figure 12. LCC comparison between the proposed and the reference methods (multiples of C_o).

According to the analysis results, the stiffness has the largest impact on LCC followed by the strength and the ductility, for the example structures. The effect of stiffness is more pronounced in the case of the 8-story structure because it has the smallest stiffness among the example structures, which makes the largest difference in stiffness with respect to the BRM.

Considering the basic assumption under which the procedure is proposed, some future work is needed to extend the proposed procedure to irregular buildings, buildings with higher mode effects, non-building structures, the inclusion of soil-structure interaction, etc. It is assumed in the current study that the investigated buildings are sensitive to displacement rather than acceleration. In other types of structures, such as offshore or industrial structures, acceleration-sensitive components may exist and acceleration needs to be included as one of the engineering demand parameters. Nevertheless, the agreement between the proposed and the reference methods is generally adequate considering the simplicity with which the LCC is estimated. Recognizing that there is a tradeoff between maintaining the required accuracy and achieving simplicity, the proposed method seems to provide a reasonable LCC estimation suitable for the preliminary design of framed structures.

The parameterized LCC procedure provides a rapid estimate of LCC which can be used for the selection of proper retrofitting options based on stiffness, strength, and ductility of the retrofitted structure. In addition, the proposed parameterized LCC enables structural engineers to practically investigate the LCC of a large number of structural options without intensive simulation. Furthermore, the parameterized LCC can be considered in the early design stage of the structure as a parameter of design and can be implemented in building design guidelines.

5. Conclusions

In this study, a new analytical LCC assessment framework was proposed based on fundamental structural characteristics such as stiffness, strength, and ductility. In the proposed method, LCC is calculated for a basic reference model (BRM) with assumed values of stiffness, strength, and ductility. Using the demand hazard and the BRM capacity curves, the inelastic spectral displacements are calculated. The dispersion measure in demand $\beta_{D|s_a}$ can be obtained based on the mean-plus-one-standard deviation response spectrum. The structural capacity uncertainty is reasonably assumed based on previous studies.

Table 4. Difference in LCC due to the difference in stiffness between the BRM and the TS.

Story number	T_{BRM} (sec)	T_{TS} (sec)	LCC for T_{BRM} (multiples of C_o)	LCC for T_{TS} (multiples of C_o)	Difference in LCC due to stiffness (multiples of C_o)
3st	1	1.5	1.463	2.321	+0.858
5st		2.07	1.169	2.164	+0.995
8st		3.15	1.085	2.642	+1.557

Table 5. Difference in LCC due to the difference in strength between the BRM and the TS.

Story number	IO used for BRM (%)	BRM strength ratio adjusted to the TS	IO used for TS (%)	TS strength ratio	LCC for IO_{BRM} (multiples of C_o)	LCC for IO_{TS} (multiples of C_o)	Difference in LCC due to strength (multiples of C_o)
3st	1.0	0.200	1.7	0.41	2.321	1.613	−0.708
5st		0.102	2.2	0.34	2.164	1.433	−0.731
8st		0.034	1.97	0.20	2.404	1.568	−0.818

Table 6. Difference in LCC due to the difference in ductility between the BRM and the TS.

Story number	$S_{din2500BRM}$ (cm)	BRM ductility factor	$S_{din2500TS}$ (cm)	TS ductility factor*	LCC for $S_{din2500BRM}$ (multiples of C_o)	LCC for $S_{din2500TS}$ (multiples of C_o)	Difference in LCC due to ductility (multiples of C_o)
3st	30.2	2.2	47.6	3.53	1.463	1.968	+0.505
5st			60.6	4.50	1.169	1.514	+0.345
8st			84.0	6.22	1.085	1.451	+0.366

*Relative to the BRM yield drift (13.5 cm, assumed as 1.0% of the H = 13.5m).

In the sequence, the limit state probability and LCC are obtained, and the graphs that relate LCC with stiffness, strength, and ductility are constructed. The target structure's fundamental response quantities are compared with those of the BRM. Using the LCC graphs and the differences in the fundamental response quantities, the LCC of the target structure can be calculated. The proposed methodology is suitable for regular low to mid-rise building configurations. Only the LCC of the BRM needs to be estimated once, and then the LCC of any building can be estimated without recourse to further simulation for each building case. In addition, the application of the method can be analytical or graphical.

The proposed parameterized LCC evaluation procedure was verified through an application on three different moment frames, and the results were compared with the results of a more rigorous method using non-linear time history analysis. The comparison revealed quite a good agreement between the results obtained by the proposed procedure and the more rigorous one. The difference as a percentage of the initial cost was found to be 2.4%, 11.9%, and 5.9%, respectively, for the 3, 5, and 8-story buildings. The proposed parameterized LCC provided an upper bound for the LCC estimation for the selected case studies. In addition, it was found that structures with small stiffness provide larger LCC than those of large stiffness. On the other hand, the increase in the strength ratio of the structure resulted in a decrease in LCC. However, the increase in the structure ductility factor caused an increase in LCC. In the current study, the effect of stiffness was found to have the largest impact on LCC followed by strength and ductility.

Based on the analysis results of the three structures investigated, it was concluded that the method is easy to implement and the results are reliable considering the assumptions and limitations mentioned, which makes it an attractive tool for LCC evaluation and assessment for existing or new structures. However, it needs to be mentioned that there are some limitations to the proposed LCC procedure to be effective. For example, the structure should be regular and low to mid-rise moment-resisting frame system. In addition, the cost related to each limit state is arbitrally assumed for simplicity.

Disclosure statement

No potential conflict of interest was reported by the author(s).

Funding

This research was carried out by research funding (task number 19CTAP-C153076-01) of the Ministry of Land, Infrastructure and Transport, Land Transport Technology Promotion Research Project.

References

ASCE/SEI 41. (2013). *Seismic evaluation and retrofit of existing buildings*. Reston, VA, USA: American Society of Civil Engineers.

Aslani, H., & Miranda, E. (2005). Probability-based seismic response analysis. *Engineering Structures*, *27*(8), 1151–1163. eng. struct. doi: 10.1016/j

ATC 40. (1996). *Seismic evaluation and retrofit of concrete buildings* (ATC 40 Report). CA, USA: Applied Technology Council.

Behrouz, B. (2019). Seismic design of steel moment-resisting structures based on life-cycle cost. *Proceedings of the Institution of Civil Engineers - Structures and Buildings*, *172*(8). 10.1680/jstbu.18.00228.

Biondini, F., & Frangopol, D.M. (2016). Life-cycle performance of deteriorating structural systems under uncertainty. *Journal of Structural Engineering*, *142*(9). doi:10.1061/(ASCE)ST.1943-541X.0001544

Bojórquez, J., Ruiz, S. E., Ellingwood, B., Reyes-Salazar, A., & Bojórquez, E. (2017). Reliability-based optimal load factors for seismic design of buildings. *Engineering Structures*, *151*, 527–539. doi:10.1016/j.engstruct.2017.08.046

Chopra, A. K. (2007). *Dynamics of structures-theory and application to earthquake engineering* (3rd ed.). NJ: Prentice Hall.

Cornell, C. A., Jalayer, F., Hamburger, R. O., & Foutch, D. A. (2002). Probabilistic basis for the 2000 SAC Federal Emergency Management Agency steel moment frame guidelines. *Journal of Structural Engineering*, *128*(4), 526–533. doi:10.1061/(ASCE)0733-9445(2002)128:4(526)

Del Gobbo, G.M., Williams, M.S., & Blakeborough, A. (2018). Seismic performance assessment of Eurocode 8-compliant concentric braced frame buildings using FEMA P-58. *Engineering Structures*, *155*, 192–208.

El-Khoury, O., Shafieezadeh, A., & Fereshtehnejad, E. (2018). A risk-based life cycle cost strategy for optimal design and evaluation of control methods for nonlinear structures. *Earthquake Engineering & Structural Dynamics*, *47*(11), 2297–2314. doi:10.1002/eqe.3069

Esteva, L., Díaz-López, O. J., Vásquez, A., & León, J. A. (2016). Structural damage accumulation and control for life-cycle optimum seismic performance of buildings. *Structure and Infrastructure Engineering*, *12*(7), 848–860. doi:10.1080/15732479.2015.1064967

Fajfar, P., & Fischinger, M. (1988). N2 - A method for non-linear seismic analysis of regular structures. In: *Proceedings of the 9th World Conference on Earthquake Engineering*.

Fajfar, P., & Dolsek, M. (2012). A practice-oriented estimation of the failure probability of building structures. *Earthquake Engineering & Structural Dynamics*, *41*(3), 531–547. doi:10.1002/eqe.1143

Fragiadakis, M., Lagaros, N. D., & Papadrakakis, M. (2006). Performance-based multiobjective optimum design of steel structures considering life-cycle cost. *Structural and Multidisciplinary Optimization*, *32*(1), 1–11. doi:10.1007/s00158-006-0009-y

Gencturk, B. (2013). Life-cycle cost assessment of RC and ECC frames using structural optimization. *Earthquake Engineering & Structural Dynamics*, *42*(1), 61–79. doi:10.1002/eqe.2193

Gencturk, B., & Elnashai, A. S. (2012). Life cycle cost considerations in seismic design optimization of structures, structural seismic design optimization and earthquake engineering: formulations and applications. In *Structural seismic design optimization and earthquake engineering: Formulations and applications* (pp. 1–22). IGI Global. 10.4018/978-1-4666-1640-0.ch001.

Hamburger, R., Rojahn, C., & Heintz, J. (2012). *FEMA P58: Next-generation building seismic performance assessment methodology*. 15th World Conference in Earthquake Engineering. Lisbon, Portugal.

Hancock, J., Bommer, J. J., & Stafford, P. (2008). Numbers of scaled and matched accelerograms required for inelastic dynamic analyses. *Earthquake Engineering & Structural Dynamics*, *37*(14), 1585–1607. doi:10.1002/eqe.827

Iervolino, I., & Cornell, C. A. (2005). Record selection for nonlinear seismic analysis of structures. *Earthquake Spectra*, *21*(3), 685–713. doi:10.1193/1.1990199

Jeong, S. H., & Elnashai, A. S. (2007). Probabilistic fragility analysis parameterized by fundamental response quantities. *Engineering Structures*, *29* (6), 1238–1251. doi:10.1016/j.engstruct.2006.06.026

Karavasilis, T. L., Bazeos, N., & Beskos, D. E. (2006). Maximum displacement profiles for the performance based seismic design of plane steel moment resisting frame. *Engineering Structures*, *28*(1), 9–22. doi:10.1016/j.engstruct.2005.06.021

Kosič, M., Dolsek, M., & Fajfar, P. (2016). Dispersions for the push-over-based risk assessment of reinforced concrete frames and cantilever walls. *Earthquake Engineering & Structural Dynamics*, *45*(13), 2163–2183. doi:10.1002/eqe.2753

Kosič, M., Fajfar, P., & Dolsek, M. (2014). Approximate seismic risk assessment of building structures with explicit consideration of uncertainties. *Earthquake Engineering & Structural Dynamics*, *43*(10), 1483–1502. doi:10.1002/eqe.2407

Lagaros, N. D., Fotis, A. D., & Krikos, S. A. (2006). Assessment of seismic design procedures based on the total cost. *Earthquake Engineering & Structural Dynamics*, *35*(11), 1381–1401. doi:10.1002/eqe.585

Liu, M., & Mi, B. (2017). Life-cycle cost analysis of energy-efficient buildings subjected to earthquakes. *Energy and Buildings*, *154*, 581–589. doi:10.1016/j.enbuild.2017.08.056

Luco, N., & Cornell, C. A. (1998). *Effects of random connection fractures on the demands and reliability for a 3-story pre-Northridge SMRF structure*. Proceedings of 6th U.S. National Conference on Earthquake Engineering, Earthquake Engineering Research Institute, Oakland, CA, USA.

Luco, N., & Cornell, C. A. (2000). Effects of connection fractures on SMRF seismic drift demands. *Journal of Structural Engineering*, *126*(1), 127–136. doi:10.1061/(ASCE)0733-9445(2000)126:1(127)

Mirzaei, H., & Nasserasadi, K. (2019). Fast seismic life cycle cost optimization of steel moment frames to improve seismic performance. *KSCE Journal of Civil Engineering*, *23*(3):1180–1189. doi:10.1007/s12205-019-2026-6.

Newmark, N. M., & Hall, W. J. (1982). *Earthquake spectra and design. EERI Monograph Series*. Oakland, CA, USA: Earthquake Engineering Research Institute.

Noureldin, M. N., & Kim, J. (2017). Simplified seismic life cycle cost estimation of a steel jacket offshore platform structure. *Structure and Infrastructure Engineering*, *13*(8), 1027–1044. doi:10.1080/15732479.2016.1233286

Noureldin, M. N., Kim, J., & Kim, J. (2019). Optimal distribution of steel slit-friction hybrid dampers based on life cycle cost. *Advances in Structural Engineering*, *22*(1), 3–646. doi:10.1177/1369433218773487

Pandey, M. D., & Weide, J. A. M. (2017). Stochastic renewal process models for estimation of damage cost over the life-cycle of a structure. *Structural Safety*, *67*, 27–38. doi:10.1016/j.strusafe.2017.03.002

Saiidi, M., & Sozen, M. A. (1981). Simple nonlinear seismic analysis of RC structures. *ASCE Journal of Structural Engineering*, *107*(5), 937–953.

SAP2000. (2018). *Analysis reference manual. Computer and Structures*. Berkeley, CA, USA: Computers and Structures. INC.

Sullivan, T. J., Welch, D. P., & Calvi, G. M. (2014). Simplified seismic performance assessment and implications for seismic design. *Earthquake Engineering and Engineering Vibration*, *13*(S1), 95–122. doi:10.1007/s11803-014-0242-0

Vitiello, U., Asprone, D., Di Ludovico, M., & Prota, A. (2017). Life-cycle cost optimization of the seismic retrofit of existing RC structures. *Bulletin of Earthquake Engineering*, *15*(5), 2245–2271. doi:10.1007/s10518-016-0046-x

Welch, D. P., Sullivan, T. J., & Calvi, G. M. (2014). Developing direct displacement-based procedures for simplified loss assessment in performance-based earthquake engineering. *Journal of Earthquake Engineering*, *18*(2), 290–322. doi:10.1080/13632469.2013.851046

Wen, Y. K., & Kang, Y. J. (2001). Minimum building Life-cycle cost design criteria I: Methodology. *Journal of Structural Engineering*, *127*(3), 330–337. doi:10.1061/(ASCE)0733-9445(2001)127:3(330)

Zhu, J., Zhao, J., & Han, H. (2019). Life-cycle seismic risk cost simplified analysis of industrial buildings, 3rd International Conference on Architectural Engineering and New Materials (ICAENM), 1–7.